Letter

# Collective gradient sensing by dilute swimming bacteria without clustering

Tatsuro Kai,[1,*] Takahiro Abe,[1,*] Natsuhiko Yoshinaga,[2,3,4] Shuichi Nakamura,[1] Seishi Kudo,[1] and Shoichi Toyabe[1,†]

[1]*Department of Applied Physics, Graduate School of Engineering, Tohoku University, Sendai 980-8579, Japan*

[2]*WPI Advanced Institute for Materials Research, Tohoku University, Sendai 980-8577, Japan*

[3]*MathAM-OIL, AIST, Sendai 980-8577, Japan*

[4]*Department of Complex and Intelligent Systems, Future University Hakodate, Hakodate 116-2, Japan*

(Received 17 November 2022; accepted 21 August 2024; published 10 September 2024)

We characterize the taxis enhancement of swimming bacteria by collective migration without apparent clustering. We confine a dilute *Salmonella* suspension in a shallow channel and evaluate the thermotaxis response to local heating and diffusion. By combining cell tracking analysis and numerical simulation based on simple modeling, we show that the alignment interaction suppresses orientation fluctuation, strengthens migration bias, and also prevents the dispersion of accumulated population. The results show a prominent example of how a collective motion of active matter implements a biological function.

DOI: 10.1103/PhysRevResearch.6.L032061

Nearly all bacterial species implement the taxis ability to migrate along the gradient of, for example, chemicals and temperature to seek a better environment. The mechanism underlying taxis differs from species to species. Bacteria with peripheral flagella such as *Escherichia coli* and *Salmonella* exhibit biased random walk with alternative run and tumble motions [1] [Fig. 1(a)]. Signal-dependent modulation of the tumbling frequency enables taxis. However, since such trial-and-error swimming of individual cells is highly stochastic, the taxis efficacy is not expected to be high. On the other hand, it is known that bacteria suspended at high density swim collectively and exhibit rich spatiotemporal phenomena such as long-distance ordering [3,4], giant number fluctuations [3], and vortex formation [5,6] caused by interaction among cells. A question that naturally arises is how the cellular interaction affects the taxis performance.

It has been observed that taxis is enhanced with increasing cellular density in a variety of systems including dense bacteria swarming on an agar plate [7] and migrating eukaryotic cells [8,9]. The density dependence suggests that the cellular interaction affects the taxis behavior. In such systems, cluster formation is supposed to be the primary mechanism. A cluster, which effectively behaves as a large body, makes it easier to sense a gradient or even enables gradient sensing even if individuals can sense only a concentration instead of a gradient.

In contrast, it has been demonstrated that the chemotaxis performance of dilute swimming bacteria increases with the cell density at a low cell density where cluster formation is not expected [10], while a further increase in density suppresses the taxis due to collective motion. There might be a novel enhancement mechanism for dilute bacterial suspensions, where the exclusion volume effect does not dominate the interaction, but it remains elusive. This work aims to quantitatively characterize how cellular interaction modifies taxis at low cell density and clarify its mechanism. For this aim, we focus on a low-density cell suspension ($\sim$1 cell/100 $\mu$m$^2$) of *Salmonella enterica* cells, where apparent clustering is not observed. As well, we used thermotaxis, that is, the property that *Salmonella* migrate along a temperature gradient. Dynamic and local heating by laser irradiation allows us to measure the temporal dynamics of the taxis response instead of the steady behavior. This helps us to understand the detailed taxis enhancement mechanism by cellular interaction.

In a dilute system, the taxis may be evaluated based on a framework similar to that for the thermophoresis of nonactive microscopic objects [11]. Let $c(\vec{r}, t)$ be the particle density at position $\vec{r}$ and time $t$. Under a given temperature gradient $\vec{\nabla} T$, both the taxis and the thermophoretic flow of nonactive particles are phenomenologically described as

$$\vec{J} = D_{\mathrm{T}}(c) c \vec{\nabla} T - D(c) \vec{\nabla} c \tag{1}$$

in a linear-response regime. $D_{\mathrm{T}}$ and $D$ are thermodiffusion and diffusion coefficients, respectively. The balance between migration bias and diffusion quantified by the Soret coefficient $S_{\mathrm{T}} \equiv D_{\mathrm{T}}/D$ determines the efficacy of detecting the temperature gradient. Actually, if the dependence of $D_{\mathrm{T}}$ and $D$ on $c$ is negligible, we obtain the steady distribution $c \propto e^{S_{\mathrm{T}} T}$ by solving $\vec{J} = 0$. This is often the case for thermophoresis. The phoresis and the taxis have distinct origins. The thermophoresis is basically driven by the interaction between the particle surface and the solvent [12], whereas bacteria realize thermotaxis by modulating their swimming pattern based

*These authors contributed equally to this work.

†Contact author: toyabe@tohoku.ac.jp

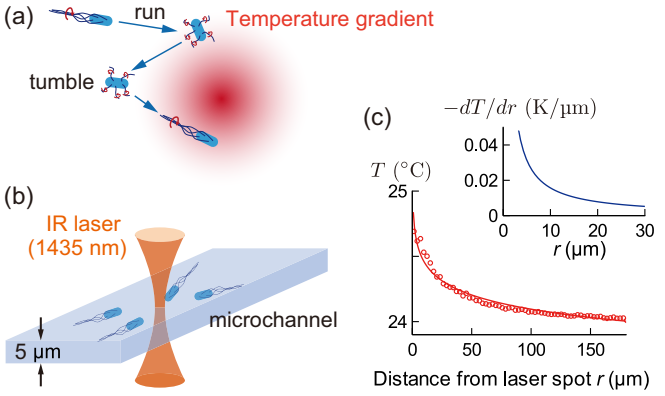


FIG. 1. Bacterial taxis. (a) Stochastic run and tumble motion realizes taxis. (b) Experimental setup. An infrared (IR) laser was focused under a microscope to generate a temperature gradient in a microchannel (Fig. S1 of the Supplemental Material [2]). (c) Temperature gradient generated by local laser heating with 200-mW power. The profile was well fitted by $a - b \ln r$, with $a = 24.8$ and $b = 0.157$. $r$ is the distance from the laser spot. The inset is the gradient calculated as $b/r$. See Fig. S4 of the Supplemental Material for details [2].

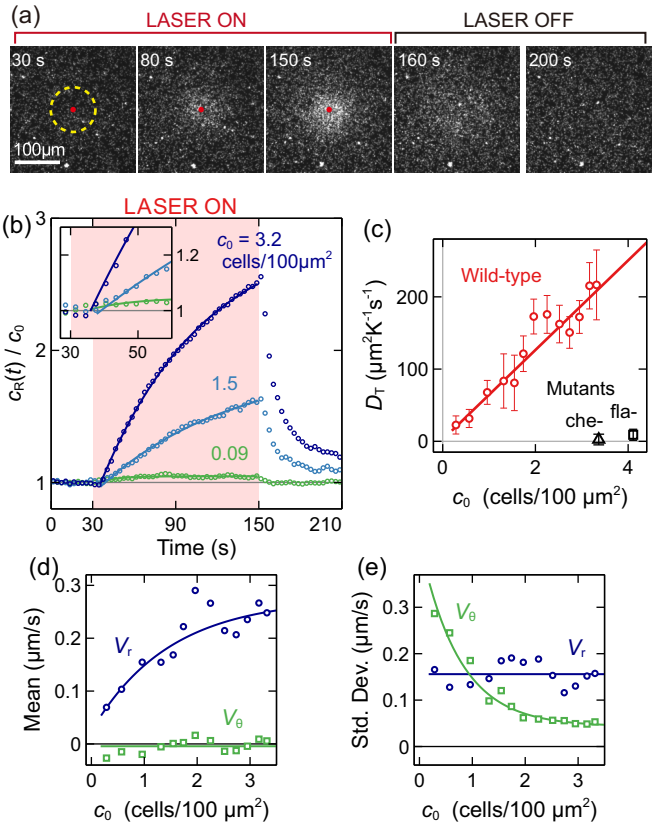


FIG. 2. Taxis to local heating. (a) The snapshots of the migration at $c_0 = 2.5$ cells/100 μm$^2$ were observed by dark-field microscopy. The red dot indicates the laser irradiation location. (b) The normalized cell density $c_R(t)/c_0$ in the central region within $R = 50$ μm (yellow dotted circle) in panel (a). $c_R(t)/c_0$ was evaluated as the ratio of the light intensity scattered by the cells under dark-field microscopy. $c_0$ was separately evaluated by identifying individual swimming cells. The data are fitted by exponential curves (solid lines) in the range between 40 and 150 s. The time profiles of 20 runs with similar $c_0$ are averaged. (c) Dependence of $D_T$ on $c_0$. The solid curve is a linear fitting. Individual observations ($N = 141$, wild-type) are sorted by $c_0$, divided into groups containing 20 data with 10 overlaps, and analyzed in each group. $N = 7$ for each mutant. The error bars indicate the standard errors. (d), (e) Single-cell tracking. The mean (d) and standard deviation (e) of radial ($V_r$) and angular ($V_\theta$) components of the velocity under the local heating averaged in the distance range between 74 and 198 μm from the heating spot and the time range of between 40 and 70 s. See Fig. S9 for the mean swimming velocity and the Method section of the Supplemental Material (SM) [2] for details. Each point is obtained from 20 runs. The solid curves are exponential or constant fittings. The plot was limited to $c_0 > 0.1$ cell/100 μm$^2$ due to limited sample number at low $c_0$.

on biochemical responses to a thermal gradient [1]. Bacteria swim ballistically at a short timescale and effectively exhibit diffusional motion only at a long timescale [1]. Despite these differences, it would still be effective to evaluate the taxis efficacy based on $D_T(c)$, the effective diffusion coefficient $D^{\rm eff}(c)$, and their ratio $S_T^{\rm eff}(c) \equiv D_T(c)/D^{\rm eff}(c)$.

We observed the swimming cells confined in a thin microchannel with a height of $h = 5$ μm, which is comparable to the cell dimensions (2–3 μm in length and ∼1 μm in width) [Fig. 1(b)]. Cells may pass each other. However, since vertical swimming is negligible, we treat the system as two-dimensional and evaluate $c$, $D_T$, and $D^{\rm eff}$ as two-dimensional quantities. Irradiation of a focused infrared laser under a microscope generated an axisymmetric pseudo-two-dimensional temperature gradient [13,14]. This setup enables the instantaneous switching on and off of the gradient for probing the taxis dynamics. The thermal convection due to the local heating was negligible because of the reduced channel height. The consumption of nutrients by cells creates a nutrient gradient and makes the dynamics complex [14,15]. We used the observation buffer lacking nutrients to focus on the effect of the cellular interaction on taxis. We also evaluated $D_T$ using the initial migration speed since cellular respiration may form the spatial oxygen gradient at a later time. The magnitude of interaction was controlled by varying the cell density.

*Results—Taxis.* The spatial temperature profile under local laser heating was well fitted by a logarithmic function as expected from the two-dimensional open system with a single heat source [16] [Fig. 1(c)]. The maximum temperature increase was about 0.7 K.

The cells migrated along the temperature gradient $\vec{\nabla} T$ and accumulated in the vicinity of the heating spot (Figs. 2(a) and S7 [2]), indicating $D_T > 0$ under the present condition. The cells dispersed when the laser was turned off. The mutant strains without flagella (fla−) or Che system (che− [17]) did not accumulate significantly (Fig. S8). The che− strain produces an intact flagellar apparatus but rotates its motors exclusively counterclockwise without tumbling. Hence, the migration originates in the taxis, not in the optical-tweezers effect [18] or the thermophoresis [11].

Let $c_R(t)$ be the mean cell density in the vicinity of the heating spot (the region within $R = 50$ μm) and $c_0$ be the mean cell density in the same region before the laser is turned on. $c_0$

was typically on the order of 1 cell/100 μm$^2$. The normalized cell density $c_R(t)/c_0$ increased linearly with a short time delay and saturated with the timescale of ∼80 s [Fig. 2(b)]. The short delay was supposedly caused by the response delay of individual cells and the large $R$ we used.

The increase in $c_R$ should equal the influx through the region's boundary. The magnitude of the influx is obtained by integrating the radial component $J_r$ of $\vec{J}$ at the periphery, $\dot{c}_R = 2\pi R J_r/\pi R^2$. Initially, $|\vec{\nabla}c|$ is negligible because of the uniform cell density. Hence, Eq. (1) is reduced to $\vec{J} = D_{\rm T} c \vec{\nabla} T$, which leads to $\dot{c}_R = 2D_{\rm T} c_0 |\vec{\nabla}T|_R/R$. Here, $|\vec{\nabla}T|_R = 0.0031$ K/μm is the temperature gradient at $R$. Thus, we can evaluate $D_{\rm T}$ as $D_{\rm T} = \alpha \dot{c}_R(t_0)/c_0$, with $\alpha = 0.5R/|\vec{\nabla}T|_R = 8.0\times10^3$ μm$^2$ K$^{-1}$. Here, $t_0 = 30$ s is the time that the laser irradiation starts. We fitted the time profile of $c_R(t)$ during heating by an exponential curve and evaluated $\dot{c}_R(t_0)$. We excluded the first 10 s during heating from the fitting range to remove the effect of the short time delay of $c_R(t)$ rising. We found that $D_{\rm T}$ increases with $c_0$. Since the increase in $c_0$ increases the contact frequency of cells, the results imply that the cellular interaction enhances taxis [Fig. 2(c)].

For further characterization of migration dynamics, we tracked individual cells and evaluated the radial ($V_{\rm r}$) and angular ($V_\theta$) components of the swimming velocity under the temperature gradient [Figs. 2(d) and 2(e)]. Since it was not feasible to track all the cells due to their overlaps, the analysis was limited to a subset of the entire population. The mean of $V_{\rm r}$ increases with $c_0$ while the standard deviations of $V_\theta$ decrease with $c_0$. In contrast, the mean swimming velocity does not significantly change with $c_0$ (Fig. S9). These results imply that the cellular interaction strengthened the directional bias toward the heating spot by aligning the swimming direction without affecting the swimming speed. Reliable evaluation of $D_{\rm T}$, $V_r$, and $V_\theta$ at vanishing $c_0$, which should converge to the taxis of a single cell, is challenging and was not possible in the present experiments due to poor statistics.

*Results-Cellular interaction.* The above results indicate that cellular interaction enhances the taxis. To characterize the interaction, we analyzed the swimming trajectories used in Figs. 2(d) and 2(e) and evaluated the collision angles $\theta_{\rm in}$ and $\theta_{\rm out}$ and their difference $\Delta\theta = \theta_{\rm out} - \theta_{\rm in}$ in the absence of a thermal gradient (Fig. 3) [4,19–21].

The cells aligned after collisions with $\theta_{\rm in} < 45^\circ$ and did not significantly align otherwise. Such mixed asymmetric interaction of polar and nematic types has been observed for the binary collision of the objects that can pass each other [21].

*Results-Diffusion.* Next, we evaluated how the modulation of diffusion by cellular interaction affects the taxis. After the laser was turned off, the cells dispersed quickly in an exponential manner [Fig. 2(b)]. The time constant of the dispersion $\tau_{\rm dis}$ increased with $c_R$ at the timing of laser off (Fig. S10 in the SM [2]). We expect $\tau_{\rm dis}$ to be independent of the density for passive Brownian particles unless the particles are extremely dense. The result implies that the cellular interaction modulates diffusion. However, the tendency of the dispersion rate to decrease with $c_0$ is opposite to the taxis enhancement $c_0$ seen in Fig. 2, where cells move in a similar direction toward the heating spot.

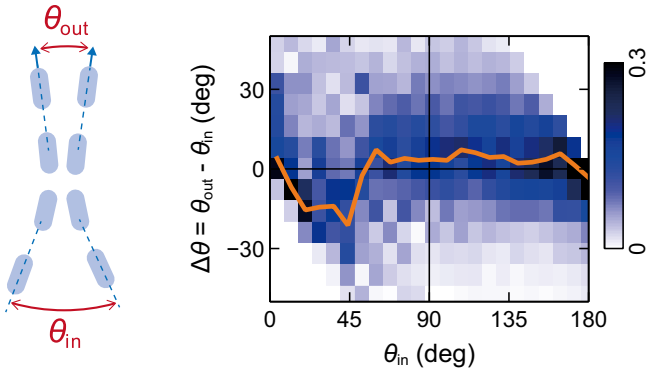


FIG. 3. Alignment interaction quantified by the angular displacement by collision. We used the same data as those in Fig. 4 ($h = 5$ μm and $c_0 < 1.5$ cells/100 μm$^2$). We analyzed 11 823 events where two cells came to close in a distance less than 2.2 μm. See SM [2] for the details. The color intensity indicates the frequency of the collision events normalized in each column. The solid line indicates the peak locations of the skewed normal distributions fitted in each column.

For more characterization, we tracked the diffusion of individual cells without laser heating. We mixed cells expressing green fluorescent protein (GFP) to track a long trajectory at high cell density. We first measured $c_0$ by counting cells in phase-contrast observation and then quantified the diffusion using the GFP cells in the same observation area in succession.

The run and tumble motion generated ballistic and diffusive motions at short and long time scales, respectively [Figs. 4(a) and 4(b)]. Trajectories became more diffusive at higher $c_0$, implying that the cellular interaction modulated the swimming pattern.

The mean square displacement (MSD), $M(\Delta t) \equiv \langle|\vec{r}(t+\Delta t) - \vec{r}(t)|^2\rangle_t$, characterizes the diffusion [Fig. 4(b)]. Here, the average $\langle\cdot\rangle_t$ is taken for different $t$. The effective diffusion coefficient $D^{\rm eff}$ is defined in the long $\Delta t$ limit as $D^{\rm eff} = \lim_{\Delta t\to\infty} M(\Delta t)/4\Delta t$ in two-dimensional systems. Since trajectories accessible by experiments are relatively short, we exploited a model fitting for estimating $D^{\rm eff}$. The MSD of a self-propelled particle with random directional change is described by

$$M(\Delta t) = 2v^2\tau[\Delta t - \tau(1 - e^{-\Delta t/\tau})] \qquad (2)$$

for a broad range of systems [22–24], including a run-and-tumble motion. Here, $v$ is the swimming velocity, and $\tau$ is the mean duration between successive direction changes. In the present system, the change in direction is supposed to be caused by the tumbling and the cellular interaction. At large $\Delta t$, $M(\Delta t) \simeq 2v^2\tau\Delta t$, which yields $D^{\rm eff} = v^2\tau/2$. We fitted $M(\Delta t)$ by Eq. (2) to obtain $D^{\rm eff}$.

$D^{\rm eff}$ decreased with $c_0$ as expected from the increase in diffusive motions. $\tau$ significantly decreased with $c_0$, whereas clear dependence of $v$ on $c_0$ was not observed (Fig. S11 [2]). Thus, the cells change directions more frequently at higher $c_0$. The result is consistent with the extended dispersion time after the laser is off at high cell density (Fig. S10 [2]). Once accumulated, the cells disperse slowly due to the slow diffusion caused by cell-cell interaction. These results indicate that

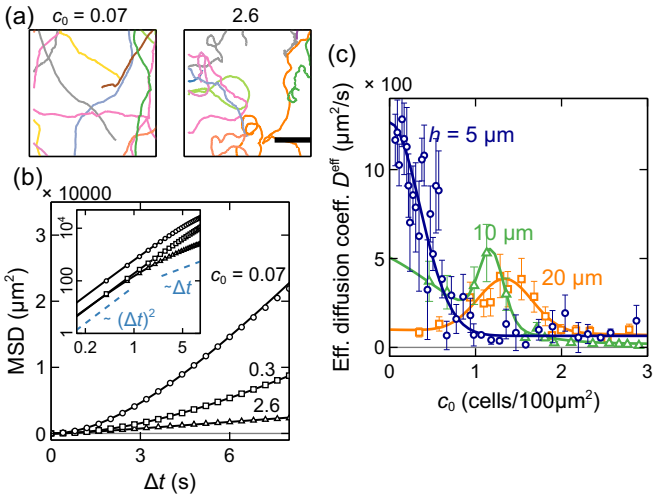


FIG. 4. Diffusion in the absence of temperature gradient. (a) Two-dimensional trajectories in the chamber with the height of $h = 5$ μm. The scale bar indicates 100 μm. (b) The mean square displacement (MSD) curve in the chamber with a height of $h = 5$ μm. The values of $c_0$ are indicated in the unit of cells/100 μm$^2$. The inset is the log-log plot. See Fig. S12 in the SM [2] for the plots with error bars. (c) Effective diffusion coefficient $D^{eff}$. The solid curves are fitting curves (see Sec. VI of SM [2]). The numbers of independent observations are 389, 120, and 192 for $h = 5$, 10, and 20 μm, respectively. The runs sorted by $c_0$ are divided into groups of 10 ($h = 5$ μm), 8 (10 μm), or 12 (20 μm) runs and analyzed collectively in each group. The error bars indicate the standard errors.

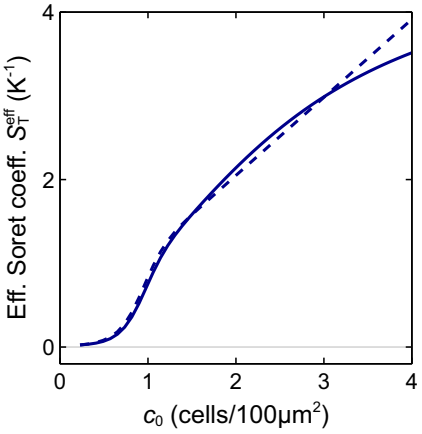


FIG. 5. Effective Soret coefficient $S_T^{eff} = D_T/D^{eff}$ in the 5-μm chamber calculated based on the fitting curves of Figs. 2(c) and 4(c).

the taxis enhancement by cell interaction is caused by both the increased migration bias and suppressed diffusion at the accumulated region.

We also measured $D^{eff}$ in thicker channels with $h = 10$ and 20 μm as the references. At small $c_0$, $D^{eff}$ decreased with $h$. It is possible that the confinement to a shallow channel suppresses the directional change and enhances the speed. Interestingly, we observed nonmonotonic dependence of $D^{eff}$ on $c_0$ in the 10- and 20-μm channels [Fig. 4(c)]. Such a peak was previously observed, but its mechanism has remained unclear [25].

This characteristic may be explained as follows. The alignment interaction suppresses the directional fluctuations and enhances the ballistic motion, which increases $D^{eff}$. However, at high $c_0$, due to the frequent collisions among cells and long-range hydrodynamic interaction, the correlated swimming may be destabilized. The balance between the alignment and the destabilization may shape the peak of $D^{eff}(c_0)$. In the thick channels, cells can easily pass each other, and the destabilization will not be effective unless $c_0$ is very large. Therefore, the peak position may shift to a large $c_0$ region. Note that, due to the limited focal depth, $c_0$ in 10- and 20-μm channels may be underestimated. However, this does not qualitatively affect the conclusion.

*Results—Coefficient.* The effective Soret coefficient $S_T^{eff} = D_T/D^{eff}$ increases steeply when $c_0$ exceeds a threshold cell density $c_0^* \sim 1$ cell/100 μm$^2$ (Fig. 5). The mean free path at $c_0^*$ is roughly estimated as $\lambda^* = 1/(2dc_0^*) \sim 50$ μm, where $d = 1$ μm is the typical cell width. $\lambda^*$ is comparable to the size of the heating region [Fig. 1(c)]. This is reasonable because the collective taxis enhancement is not expected if cells do not interact during the migration toward the hot region. The actual value of $\lambda^*$ should be larger because cells can pass each other even in the present thin chamber. However, $\lambda^*$ will still be comparable to the heating-spot size.

*Results—Simulation.* For elucidating the mechanism of the taxis enhancement, we modeled the cells as self-propelled spherical particles and performed numerical simulations (Fig. 6) [26–30]. See SM (Sec. VII) for details [2]. The

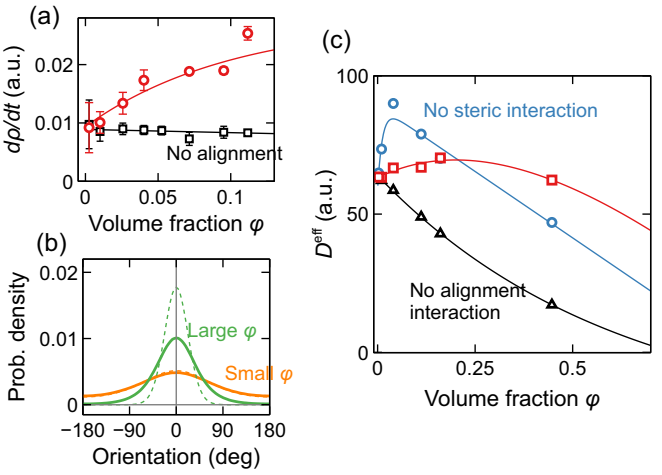


FIG. 6. Simulation. (a) Response to a Gaussian-shaped axisymmetric external field. $d\rho/dt$ is the rate of increase of the density $\rho$ within the region around the center (see the SM [2] for details). The solid curves are exponential fitting. (b) Steady distribution of velocity orientation obtained by simulations (solid lines) and mean-field approximation (dashed lines, see Eq. (S11) in the SM [2]). A uniform external field is induced in the direction of $\theta = 0$. $\varphi = 0.11$ (green curves) or 0.0025 (orange curve). See the SM (Sec. VIIB [2]) for the definition of the response to an external field. (c) Effective diffusion coefficient with or without steric repulsion and polar interaction. The solid curves are exponential + linear (blue and red curves) or exponential (black curves) fitting. See also Fig. S6 in the SM [2] for the effective Soret coefficient.

particles translated with a constant velocity and changed their swimming direction by the interaction with other particles as well as rotational fluctuation with white Gaussian statistics. The interaction included the short-range repulsion, which modeled the excluded volume effect, the polar interaction, which aligned the swimming direction of nearby cells, and the long-range hydrodynamic interaction, in which the cells were modeled as pushers. We also included the driving by an external field for measuring response.

The simulations qualitatively reproduced the taxis and diffusion observed in the experiments despite the simplicity of the model (Fig. 6). Specifically, the response to a Gaussian-shaped external field increased with the initial particle density measured by the volume fraction $\varphi$ [Fig. 6(a)]. Such density dependence was not observed without alignment interaction. When a uniform external field was imposed, the steady distribution of the orientation became steeper with $\varphi$ [Fig. 6(b)]. This result reproduced the experimental results that the mean of the drift velocity increased and its variance decreased [Figs. 2(d) and 2(e)], validating the hypothesis that the alignment interaction enhances the migration bias and suppresses the rotational diffusion.

The peak of $D^{\mathrm{eff}}$ observed in experiments [Fig. 4(c)] was also reproduced by simulation [Fig. 6(c)]. Without the alignment interaction, $D^{\mathrm{eff}}$ monotonically decreased, validating that the cellular alignment enhances the diffusion. The peak of $D^{\mathrm{eff}}$ was large without the excluded volume effect, where the particles can slip through others. This situation models the experiments with thick chambers, in which we observed prominent peaks [Fig. 4(c)]. Let the volume of a single cell be $V = 3\ \mu\mathrm{m}^3$. A typical cell density in the experiment $c_0 = 1$ cell$/100\ \mu\mathrm{m}^2$ is converted to the volume fraction of $\varphi = 0.006$ for the $h = 5\ \mu\mathrm{m}$ channel. However, since the interaction range rather than particle size affects the cellular interaction more, it is not straightforward to compare $c_0$ and $\varphi$.

*Discussion.* Bacterial thermotaxis has been investigated since the 1970s [31–33]. The density dependence of the thermotaxis was recently studied with a focus on the effect of the cellular metabolism [14,15,34,35]. Cells' secretion and consumption of chemicals such as glycine and oxygen create a chemical gradient, which induces chemotaxis and modulates the migration. Swimming speed variation by temperature also induces a temperature-dependent diffusion and enables a thermotaxis without receptors for taxis [35].

Here, we circumvented such complications and focused on how the cellular physical interaction affects the taxis behavior. As mentioned, the collective gradient sensing of dense cells has been explained by cluster formation [7–9]. In contrast, in the present dilute system, distinct cluster formation was not observed, implying a different class of collective sensing mechanisms. Based on the experimental results, the enhanced migration bias we demonstrated here may be explained by the following mechanism. The taxis of a single cell is not effective due to strong fluctuations. However, in a bacterial suspension, cellular interaction at repetitive instantaneous contacts aligns the swimming directions of the nearby cells to their major direction and increases the sensing limit.

The taxis at vanishing cell densities, corresponding to single cell taxis, was not well resolved due to low statistics. The simulation qualitatively reproduced the enhancement of taxis by cellular interaction. Quantitatively, however, the simulation [Fig. 6(a)] shows limited taxis enhancement compared to the experiment [Fig. 2(c)]. There may be other effects not considered in the simulation. For example, there may be a static interaction between cells that enhances accumulation. We have focused here on the essence of how the alignment interaction affects the taxis. More detailed modeling is left for future studies.

*Acknowledgments.* We thank Y. T. Maeda, T. Hiraiwa, and Y. Nakayama for helpful discussions and M. Fukuyama and A. Hibara for technical assistance. This research was supported by JSPS KAKENHI (Grant No. JP18H05427 to S.T. and Grants No. JP20K03874 and No. JP24K00591 to N.Y.), JST ERATO Grant No. JPMJER2302, Japan, and Tohoku University Nanotechnology Platform sponsored by MEXT, Japan (Grant No. JPMX09F-20-TU-0083).

[1] H. C. Berg, *E. Coli in Motion* (Springer, New York, 2004).

[2] See Supplemental Material at http://link.aps.org/supplemental/10.1103/PhysRevResearch.6.L032061 for supplementary methods and figures.

[3] H. P. Zhang, A. Be'er, E.-L. Florin, and H. L. Swinney, Collective motion and density fluctuations in bacterial colonies, Proc. Natl. Acad. Sci. USA **107**, 13626 (2010).

[4] D. Nishiguchi, K. H. Nagai, H. Chaté, and M. Sano, Long-range nematic order and anomalous fluctuations in suspensions of swimming filamentous bacteria, Phys. Rev. E **95**, 020601(R) (2017).

[5] C. Dombrowski, L. Cisneros, S. Chatkaew, R. E. Goldstein, and J. O. Kessler, Self-concentration and large-scale coherence in bacterial dynamics, Phys. Rev. Lett. **93**, 098103 (2004).

[6] K. Beppu, Z. Izri, J. Gohya, K. Eto, M. Ichikawa, and Y. T. Maeda, Geometry-driven collective ordering of bacterial vortices, Soft Matter **13**, 5038 (2017).

[7] M. Tian, C. Zhang, R. Zhang, and J. Yuan, Collective motion enhances chemotaxis in a two-dimensional bacterial swarm, Biophys. J. **120**, 1615 (2021).

[8] B. A. Camley, Collective gradient sensing and chemotaxis: Modeling and recent developments, J. Phys. **30**, 223001 (2018).

[9] A. Haeger, K. Wolf, M. M. Zegers, and P. Friedl, Collective cell migration: Guidance principles and hierarchies, Trends Cell Biol. **25**, 556 (2015).

[10] R. Colin, K. Drescher, and V. Sourjik, Chemotactic behaviour of *Escherichia coli* at high cell density, Nat. Commun. **10**, 5329 (2019).

[11] R. Piazza and A. Parola, Thermophoresis in colloidal suspensions, J. Phys. **20**, 153102 (2008).

[12] J. L. Anderson, Colloid transport by interfacial forces, Annu. Rev. Fluid Mech. **21**, 61 (1989).

[13] D. Braun and A. Libchaber, Trapping of DNA by thermophoretic depletion and convection, Phys. Rev. Lett. **89**, 188103 (2002).

[14] M. Demir, C. Douarche, A. Yoney, A. Libchaber, and H. Salman, Effects of population density and chemical environment on the behavior of *Escherichia coli* in shallow temperature gradients, Phys. Biol. **8**, 063001 (2011).

[15] H. Salman, A. Zilman, C. Loverdo, M. Jeffroy, and A. Libchaber, Solitary modes of bacterial culture in a temperature gradient, Phys. Rev. Lett. **97**, 118101 (2006).
[16] Y. Sakamoto and S. Toyabe, Assembly of a functional and responsive microstructure by heat bonding of DNA-grafted colloidal brick, Sci. Rep. **7**, 9104 (2017).
[17] Y. Magariyama, S. Yamaguchi, and S. Aizawa, Genetic and behavioral analysis of flagellar switch mutants of Salmonella typhimurium, J. Bacteriol. **172**, 4359 (1990).
[18] A. Ashkin, Optical trapping and manipulation of neutral particles using lasers, Proc. Natl. Acad. Sci. USA **94**, 4853 (1997).
[19] I. S. Aranson, A. Sokolov, J. O. Kessler, and R. E. Goldstein, Model for dynamical coherence in thin films of self-propelled microorganisms, Phys. Rev. E **75**, 040901(R) (2007).
[20] T. Ishikawa, Suspension biomechanics of swimming microbes, J. R. Soc. Interface **6**, 815 (2009).
[21] R. Suzuki, C. A. Weber, E. Frey, and A. R. Bausch, Polar pattern formation in driven filament systems requires non-binary particle collisions, Nat. Phys. **11**, 839 (2015).
[22] X.-L. Wu and A. Libchaber, Particle diffusion in a quasi-two-dimensional bacterial bath, Phys. Rev. Lett. **84**, 3017 (2000).
[23] J. R. Howse, R. A. L. Jones, A. J. Ryan, T. Gough, R. Vafabakhsh, and R. Golestanian, Self-motile colloidal particles: From directed propulsion to random walk, Phys. Rev. Lett. **99**, 048102 (2007).
[24] H.-R. Jiang, N. Yoshinaga, and M. Sano, Active motion of janus particle by self-thermophoresis in defocused laser beam, Phys. Rev. Lett. **105**, 268302 (2010).
[25] M. Wu, J. W. Roberts, S. Kim, D. L. Koch, and M. P. DeLisa, Collective bacterial dynamics revealed using a three-dimensional population-scale defocused particle tracking technique, Appl. Environ. Microbiol. **72**, 4987 (2006).
[26] A. Amiri, R. Mueller, and A. Doostmohammadi, Unifying polar and nematic active matter: Emergence and co-existence of half-integer and full-integer topological defects, J. Phys. A **55**, 094002 (2022).
[27] E. Sesé-Sansa, D. Levis, and I. Pagonabarraga, Phase separation of self-propelled disks with ferromagnetic and nematic alignment, Phys. Rev. E **104**, 054611 (2021).
[28] J. Blake, Self propulsion due to oscillations on the surface of a cylinder at low Reynolds number, Bull. Aust. Math. Soc. **5**, 255 (1971).
[29] N. Yoshinaga and T. B. Liverpool, Hydrodynamic interactions in dense active suspensions: From polar order to dynamical clusters, Phys. Rev. E **96**, 020603(R) (2017).
[30] T. Hiraiwa, Dynamic self-organization of idealized migrating cells by contact communication, Phys. Rev. Lett. **125**, 268104 (2020).
[31] K. Maeda, Y. Imae, J. I. Shioi, and F. Oosawa, Effect of temperature on motility and chemotaxis of Escherichia coli, J. Bacteriol. **127**, 1039 (1976).
[32] K. Maeda and Y. Imae, Thermosensory transduction in Escherichia coli: Inhibition of the thermoresponse by L-serine, Proc. Natl. Acad. Sci. USA **76**, 91 (1979).
[33] E. Paster and W. S. Ryu, The thermal impulse response of Escherichia coli, Proc. Natl. Acad. Sci. USA **105**, 5373 (2008).
[34] H. Salman and A. Libchaber, A concentration-dependent switch in the bacterial response to temperature, Nat. Cell Biol. **9**, 1098 (2007).
[35] M. Demir and H. Salman, Bacterial thermotaxis by speed modulation, Biophys. J. **103**, 1683 (2012).